Application of Linear Prediction, Self-Adaptive Noise Cancellation and Spectral Kurtosis in Identifying Natural Damage of a Rolling Element Bearing in a Gearbox

Cristóbal Ruiz-Cárcel, Enrique Hernani-Ros, Yi Cao, Michael Corsar and David Mba

School of Engineering, Cranfield University (UK); Building 52, Cranfield University, Bedfordshire, MK43 0AL, UK

Pramesh Chandra

Moog Aircraft Group, Wolverhampton (UK), Wobaston Road, Wolverhampton, WV9 5EW, UK

(Received 20 September 2012; revised 17 December 2013; accepted 26 February 2014)

The ability to detect and diagnose faults in rolling element bearings is crucial for modern maintenance schemes. Several techniques have been developed to improve the ability of fault detection in bearings using vibration monitoring, especially in those cases where the vibration signal is contaminated by background noise. Linear Prediction and Self-Adaptive Noise Cancellation are techniques which can substantially improve the signal to noise ratio of the signal, improving the visibility of the important signal components in the frequency spectrum. Spectral Kurtosis has been shown to improve bearing defect identification by focusing on the frequency band with a high level of impulsiveness. In this paper the ability of these three methods to detect a bearing fault is compared using vibrational data from a specially designed test rig that allowed fast natural degradation of the bearing. The results obtained show that the Spectral Kurtosis was able to detect an incipient fault in the outer race of the bearing much earlier than any other technique.

NOMENCLATURE

$a(k)$	Weight attached to each observation in LP
ANC	Adaptive Noise Cancelling
e	Output in ANC and SANC
f	Frequency
GM	Gear mesh frequency
H	Filter length
IRD	Inner race defect frequency
K	Kurtosis
LF	Line Frequency
LP	Linear prediction
n	Time point
N	Number of past samples considered in the calculation of R_τ
n_0	Reference noise
n_1	Uncorrelated eference noise
ORD	Outer race defect frequency
p	Number of past samples considered in LP
R_τ	Autocorrelation function
S	Signal of interest in ANC/SANC
SAN	Self-Adaptive Noise Cancellation
SK	Spectral Kurtosis
SNR	Signal to Noise Ratio
SS	Shaft speed frequency
W	Vector of filter coefficients
w	Filter weights in ANC and SANC
x	Random signal
$\hat{x}(n)$	Predictable part of signal x at
$y(n)$	Filter output
Δ	Time delay
Δf	Frequency band width
μ	Forgerring factor
μ	Average value
σ	Standard deviation

1. INTRODUCTION

Rolling element bearings are important components in rotating machinery. By monitoring the vibration signature of bearings, it is possible to obtain important information about their condition and use this information to improve the maintenance strategy. Diagnostic techniques based on vibration are mainly concerned with the extraction of defect features in the acquired signal, which can be related to the healthy or defective state of vital parts in a machine. Many different diagnostic methods have been successfully used to identify machine faults, processing the vibration signal in the time or frequency domain, in order to locate and quantify any existing damage. In complex machines the signal acquired is normally inclusive of additive background noise from other machine components or subsystems, which can make it difficult or sometimes impossible to identify the fault patterns in the signal.

In the case of bearings, the fault is produced typically by the damage of the surface of the inner or outer race or the rolling elements. When a damaged surface contacts another rolling surface, a force impulse is generated, which excites resonances in the bearing and the machine.[1] The successive impacts generate a vibration signal, which often has an impulsive repeti-

tive nature that is easy to identify in the presence of low background noise. In a real machine, the background noise can mask the bearing fault components of the signal, especially in gearboxes because the gear meshing can generate a strong level of vibration.[2] For this reason, many different methodologies of signal processing have been developed in order to facilitate the detection of defects, particularly in bearings.

Some examples of classic techniques used to enhance bearing fault features in vibration signals are linear prediction (LP), self-adaptive noise cancellation (SANC), cyclostationarity, Hilbert-Huang transform (HHT), and wavelet transform (WT). LP is based on the estimation of the deterministic part of a signal as a linear combination of the past inputs and outputs of the system, while SANC aims to minimize the noise in the manipulated signal by recursively adapting the filtration parameters.[3] Cyclostationarity studies the periodicities of the different features of machine vibration signals using the cyclic autocorrelation function and spectral correlation density.[4] HHT can be used to decompose a non-stationary and nonlinear signal into intrinsic mode functions and obtain instantaneous frequency data,[5] and WT can be applied on non-stationary signals to increase the frequency resolution at low frequencies and reduce noise in raw signals.[6] All of these techniques have been already applied by various researchers for the detection and diagnosis of bearing and gearbox faults.

In this investigation, three diagnostic techniques, LP, SANC and SK were applied in identifying a bearing defect in a gearbox where the bearing degradation happened naturally in a specially designed test rig. LP and SANC have been successfully used as de-noising tools in different applications for many years.[7,8] Nevertheless, even nowadays many researchers are exploring their capabilities to reduce background noise and enhance the fault features in a signal to improve the fault detection and diagnosis in bearings.[9–15] On the other hand, SK is a relatively new methodology that is able to enhance the fault signature in a signal by focusing in the frequency band with a higher level of impulsiveness.[16–18] This technique has been demonstrated to be very effective, especially for bearing fault detection, and many researchers have reported its benefits.[19–24]

The aim of this paper is to compare the performance of these methodologies in detecting a bearing fault during the early stages of natural degradation and show the benefits of SK over more stablished denoising techniques. For this purpose, these three methodologies have been applied on a vibrational signal acquired from a particular gearbox where the bearings failed much earlier than the theoretical life calculated for the loading conditions. Analysis of acquired vibration signals associated with different stages of bearing degradation proved to be ideal for this comparative study. This was principally because the bearing defect frequency was only evident at the final stage of degradation. Thus, the study presented will explore whether or not these techniques can offer the ability to identify the presence of the defect earlier.

2. THEORETICAL BACKGROUND

2.1. Linear Prediction

The estimation of a dynamic system output and its later analysis is one of the most important problems in signal processing. Different techniques have been employed by several researchers in a wide range of applications such as neurophysics, electrocardiography, geophysics, and speech communication.[7] One of the most powerful estimation models is based on the assumption that the value of a signal x at the time n can be obtained as a linear combination of past inputs and outputs of the system. Those models which use the information from only the past system outputs are called all-pole or autoregressive models, and were first used by Yule in an investigation of sunspot numbers.[25] LP is one of those methods where the objective is to predict or estimate the future output of a system based on the past output observations. The complete mathematical development and a compilation of the different LP approaches have been presented by Makhoul.[7]

In vibration-based diagnostics, LP is a method that allows the separation of the deterministic or predictable part of a signal from the random background noise using the information provided by past observations.[14,26] If it is assumed that the background noise is totally random, by applying this method, it is possible to eliminate the background noise and thus improve the signal-to-noise ratio. This technique is based on the principle that the value of the deterministic part of a signal can be predicted as a weighted sum of a series of previous values:

$$\hat{x}(n) = -\sum_{k=1}^{p} a(k) \cdot x(n-k); \tag{1}$$

where $\hat{x}(n)$ is the predictable part of the n$^{\text{th}}$ sample of the signal x, p is the number of past samples considered, and $a(k)$ are the weights attached to each past observation. The weighting coefficients can be obtained at each step, n, by a linear operation from the autocorrelation function R_τ of the time series $x(n)$, which can be efficiently solved using the Yule-Walker equation:[27]

$$\begin{bmatrix} R_0 & R_1 & \cdots & R_{p-1} \\ R_1 & R_0 & \cdots & R_{p-2} \\ \vdots & \vdots & \ddots & \vdots \\ R_{p-1} & R_{p-2} & \cdots & R_0 \end{bmatrix} \cdot \begin{bmatrix} a_1 \\ a_2 \\ \vdots \\ a_p \end{bmatrix} = \begin{bmatrix} -R_1 \\ -R_2 \\ \vdots \\ -R_p \end{bmatrix}; \tag{2}$$

where,

$$R_\tau = \frac{1}{N} \sum_{t=\tau}^{N} x(t-\tau) \cdot x(t). \tag{3}$$

N is the number of past samples considered at each step, in this case only p past samples were considered for each $\hat{x}(n)$ prediction for computational reasons, but all the available past samples at each time point were used in the calculation of the values R_τ.

The results of the algorithm depend on the number of past observations p considered. Small values of p produce a poor prediction, giving a result of negligible improvement in the signal-to-noise ratio, while very high values of p affect the computational cost negatively, over restrain the prediction, and tend to reduce even the main components of the signal. For this particular investigation, several analyses were carried out using different numbers of past samples in order to establish the value p for each test case, which optimizes the signal-to-noise ratio of the output signal.

2.2. Self-Adaptive Noise Cancellation

Adaptive noise cancelling (ANC) is another technique used to reduce the background noise in a signal and increase the

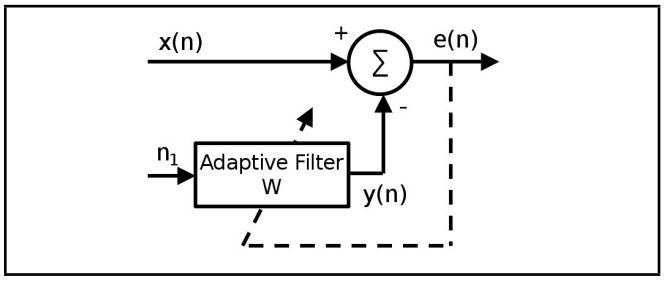

Figure 1. ANC algorithm.

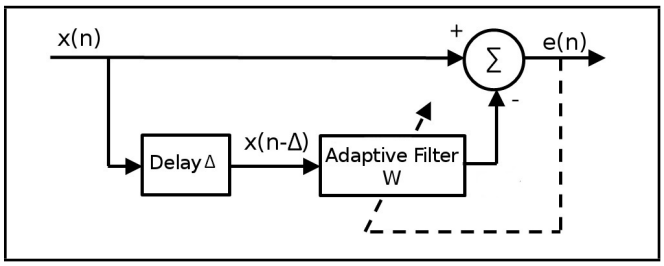

Figure 2. SANC algorithm.

signal-to-noise ratio, improving the visibility of the different signal components in the frequency spectrum. The first work in ANC was performed by Howells and Applebaum at the General Electric Company between 1957 and 1960. The first ANC system was designed and built at Stanford University in 1965.[8] Since then, this method has been successfully applied to a number of additional problems including electrocardiography, cancelling noise in speech signals, cancelling antenna sidelobe interferences, etc.[8]

The general ANC concept is shown in Fig. 1, and a basic explanation of the method was given by Chaturvedi et al.:[28] the input $x(n)$ composed by the signal of interest S and additive noise n_0 is received at the primary sensor. A reference noise n_1 (which must be related to the noise n_0 in some unknown way but is not coherent with the signal S) is received at the reference sensor. The reference input is then adaptively filtered to match n_0 as closely as possible, which is then subtracted from the primary input $x(n) = S + n_0$ to produce the system output $e = S + n_0 - y$. This output contains the signal plus residual undesirable noise. The adaptive filter acts to minimize, indirectly, the average power of this residual noise at the system output e. The output is fed back to the adaptive filter, and the filter weights are adjusted at each calculation step to minimize the total output power of the system. It can be demonstrated that minimizing the total output power minimizes the output noise power or, in other words, maximizes the output signal-to-noise ratio.[8]

The problem of this method applied to bearing fault detection in real applications is that it is not always easy to identify the source of noise n_1, which is correlated with the noise n_0 (common source) but not with the fault signal. Chaturvedi et al.[28] presented an example where the method was applied to detect an induced bearing fault in a gearbox using two sensors; one was placed in the surroundings of the bearing housing to obtain the main signal, and another sensor was placed at a remote location in the casing of the gearbox to obtain the reference signal. To solve this issue, a further development of ANC was formulated using a delayed version of the primary signal.[8] This latter version was named the self-adaptive noise cancellation (SANC), and the schematic concept is represented in Fig. 2. The time delay Δ, which is fixed, forces the delayed version of the input signal to become uncorrelated with the primary signal, introducing a phase difference. The adaptive filter responds firstly by compensating for the phase shift so that the sinusoidal components cancel each other at the output, and secondly by removing as much noise as possible to minimise the output error.[29] As it happens in the original ANC, the output error is then fed back to the adaptive filter to adjust recursively the filter weights w in order to minimize the total output power and thus, the output noise power. There are many adaptation rules to do this, the most well-known is the least mean square:[8]

$$w_i^{n+1} = w_i^n + \mu \cdot e(n) \cdot x(n - \Delta - i); \tag{4}$$

where the parameter μ (forgetting factor, strictly positive) controls the stability and rate of convergence of the process, and the subscript i differentiates each of the H weighting coefficients of the filter. The recursive weight calculation starts with a random value for each weight w_i. The output of the filter $y(n)$ can be calculated as:

$$y(n) = W^T(n) \cdot X(n - \Delta); \tag{5}$$

where W is a vector containing the H weighting coefficients w_i, and $X(n - \Delta)$ is another vector containing the H components of the delayed signal immediately preceding the sample n. The output $e(n)$ is easily obtained from:

$$e(n) = x(n) - y(n). \tag{6}$$

As shown by Eq. (4), the performance of the SANC algorithm clearly depends on the choice of three parameters: the time delay Δ, the filter length H, and the forgetting factor μ. The influence of these parameters was investigated by Ho et al.[30] who suggested some parameter selection guides. Δ should be large enough to ensure that the delayed signal becomes uncorrelated with the original, and H should be chosen to cancel all the broadband components of the delayed signal. In both cases, if the selected value for the parameter is too large, it will lead to computation problems. Ho[30] stated that the forgetting factor depends mainly on the filter order H. In this particular investigation, the parameters Δ, H, and μ were selected after several tests with the aim of optimizing the signal-to-noise ratio of the output signal. From these tests it was concluded that the selection of μ is crucial for the process performance: very small variations on this parameter can change the output signal, from no noise reduction effect if the selected value is too high, to distortion of the main signal components when it is too low. This influence can be seen in Fig. 3 where the SANC was applied to a representative signal acquired during the tests using different values for the forgetting factor μ. It is always important to check the convergence of the filter weights to ensure optimal performance.

2.3. Spectral Kurtosis and Envelope Analysis

Kurtosis is defined as the degree of peakness of a probability density function $p(x)$, and mathematically it is defined as the normalized fourth moment of a probability density function:[31]

$$K = \frac{\int_{-\infty}^{\infty} [x - \mu]^4 p(x) dx}{\sigma^4}; \tag{7}$$

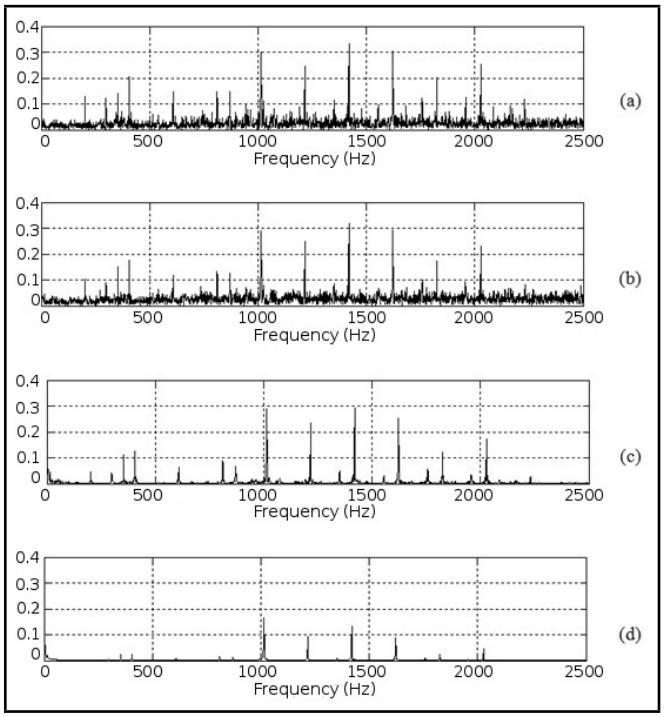

Figure 3. Effect of the forgetting factor μ on the SANC results. (a):original spectrum; (b) signal processed through SANC using $\mu = 0.0001$; (c) signal processed through SANC using $\mu = 0.00001$; (d) signal processed through SANC using $\mu = 0.000001$.

where x is the signal of interest with average μ and standard deviation σ.

As mentioned earlier, in real applications background noise often masks the signal of interest, and, as a result, the kurtosis is unable to capture the peakness of the fault signal, giving usually low kurtosis values. Therefore, in applications with strong background noise, the kurtosis as a global indicator is not useful, and it gives better results when it is applied locally in different frequency bands.[17] This technique is named spectral kurtosis (SK).

The SK was first introduced by Dwyer[32] as a statistical tool, which can locate non-Gaussian components in the frequency domain of a signal. This method is able to indicate the presence of transients in the signal and show their locations in the frequency domain. It has demonstrated to be effective even in the presence of strong additive noise.[17] The basic principle of this method is to calculate the kurtosis at different frequency bands in order to identify non stationarities in the signal and determine where they are located in the frequency domain. Obviously the results obtained strongly depend on the width of the frequency bands Δf in which the analysis is performed and its influence was analysed by Antoni.[18]

The kurtogram is basically a representation of the calculated values of the SK as a function of f and Δf.[33] However, the exploration of the whole plane (f, Δf) is a complicated computation task difficult to deal with, though Antoni[18] suggested a methodology for the fast computation of the SK. In this approach, at each bandwidth level, the number of filtered sequences is increased by a factor 2, and the kurtogram is finally estimated by computing the kurtosis of all sequences.

The importance of the kurtogram relies on the fact that it allows the identification of the frequency band where the SK is maximum, and this information can be used to design a filter that extracts the part of the signal with the highest level of impulsiveness. Antoni et al.[17] demonstrated how the optimum filter which maximizes the signal-to-noise ratio is a narrowband filter at the maximum value of SK. Therefore the optimal central frequency and bandwidth of the band-pass filter are found as the values of f and Δf which maximise the kurtogram. The filtrated signal can be finally used to perform an envelope analysis, which is a widely used technique for identification of modulating frequencies related with bearing faults. In this investigation the SK computation and the subsequent signal filtration and envelope analysis was performed using original Matlab code programmed by Jérôme Antoni.

This investigation assesses the merits of these three techniques in identifying a natural degraded bearing under conditions of relatively large background noise.

3. EXPERIMENTAL SET UP

The vibrational data used in this investigation was obtained from a specially designed gearbox test rig. The gearbox type employed is a part of the transmission driveline on the actuation mechanism of secondary control surfaces in civil aircrafts. The bearing of this gearbox failed in an endurance test at around 30% of its total expected life (around 3000 hours), making it an ideal candidate for this investigation where fast natural degradation of the bearing was needed. The rig was built originally to identify the origin of premature failure in order to modify the gearbox design. The acquired vibrational signal was used in this investigation to find traces of the fault during the early stages of degradation, which is an obvious advantage from a maintenance point of view.

This gearbox, whose basic cross section is shown in Fig. 4, has two bevel gears with 17 teeth on each gear, generating a transmission ratio of 1:1. Each gear is supported by two angular contact bearings with 12 balls each and a contact angle of 40°, mounted in a back-to-back configuration. The main dimensions of the bearing and the attached bearing defect frequencies can be seen in Table 1 and Table 2 respectively. The test rig was built trying to emulate the actual transmission system used in the aircraft, and it is schematically represented in Fig. 5. The transmission is driven by an electric motor with a nominal speed of 710 rpm. An electric load motor placed at the opposite side of the test rig was used to apply different loads used during the experiment. In order to simulate the actual loading conditions expected during the life of the gearboxes, the test rig was subjected to a mixture of seven different types of flight load cycles derived from the actual flight data and loads. These load cycles include the simulation of takeoff and landing with different flap positions, ground maintenance, etc. The expected bearing life for these loading conditions was around 3000 hours. Figure 6 shows a typical type 3 load profile, which was chosen as an illustrative example because it contains several speed changes and the highest torque is applied in this particular load cycle. The loading conditions of each cycle type applied are explained in Table 3, which specifies the number of times each cycle was applied during the experiment for the expected bearing life, the duration of each cycle, and the maximum torque applied in each case.

The experiment ran continuously for 24 hours a day over a duration of 36 days, but at certain points during the test run the rig was stopped for visual inspection for damage in the bearings. The gearbox was always then reassembled and the se-

Table 2. Main Defect Frequencies and Harmonics (Hz).

Harmonic	1X	2X	3X	4X	5X	6X
Shaft speed frequency (SS)	11.8	23.7	35.5	47.3	59.2	71
Gear mesh frequency (GM)	201.2	402	604	805	1006	1207
Inner race defect frequency(IRD)	83.2	166	250	333	416	499
Outer race defect frequency (ORD)	58.8	118	176	235	294	353
Cage defect frequency	4.9	9.8	14.7	19.6	24.5	29.4
Ball spin frequency	25.6	51.2	76.8	102	128	154
Rolling element defect frequency	51.2	102	154	205	256	307

Table 3. Load cycles characteristics summary.

Cycle type	1	2	3	4	5	6	7	8	9
Number of repetitions during bearing life	18296	22869	4574	462	462	2200	6600	4620	41580
Duration (sec)	131	131	131	350	42	71	268	52	52
Torque max. (Nm)	126.1	126.1	158.6	126.1	126.1	42.8	42.8	12.4	97.7

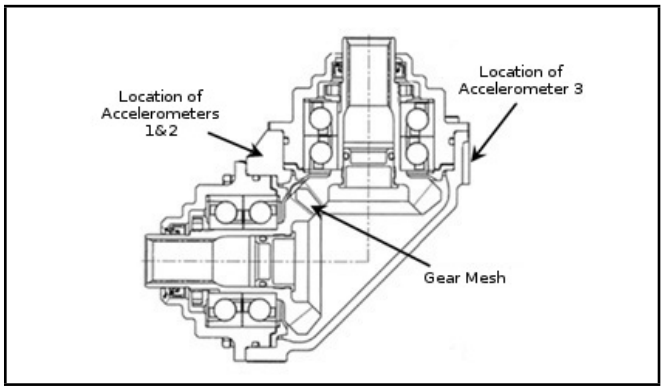

Figure 4. Gearbox Section.

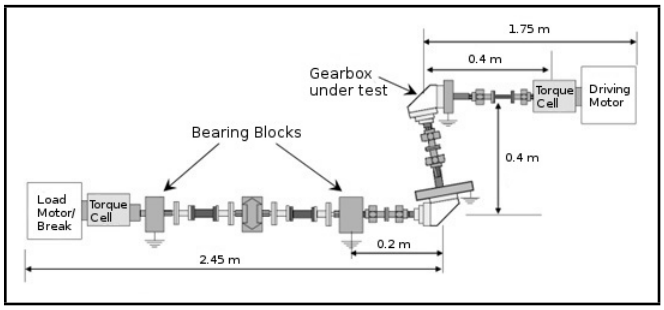

Figure 5. Layout of the test rig.

quence continued. Figure 7 shows a detail of the bearing outer race during a visual inspection undertaken one month after the experiment started, covering 24% of the estimated bearing life.

Three accelerometers were mounted in the gearbox at locations identified in Fig. 4, two of them placed on the top of the gearbox measuring acceleration in the vertical plane and a third one placed on the casing measuring the acceleration in the horizontal plane. The selected accelerometers (Omni Instruments model RYD81D) had an operating frequency range of 10 Hz to 10 kHz. These accelerometers were connected to signal conditioners (model Endevco 2775A) that were at-

Table 1. Bearing Main Dimensions.

No. of rolling elements	12
Ball Diameter (B_d)	0.4063"
Contact Angle (Φ)	40°
Pitch Diameter (P_d)	1.811"
Input Shaft Speed	710 rpm
Gear Teeth	17

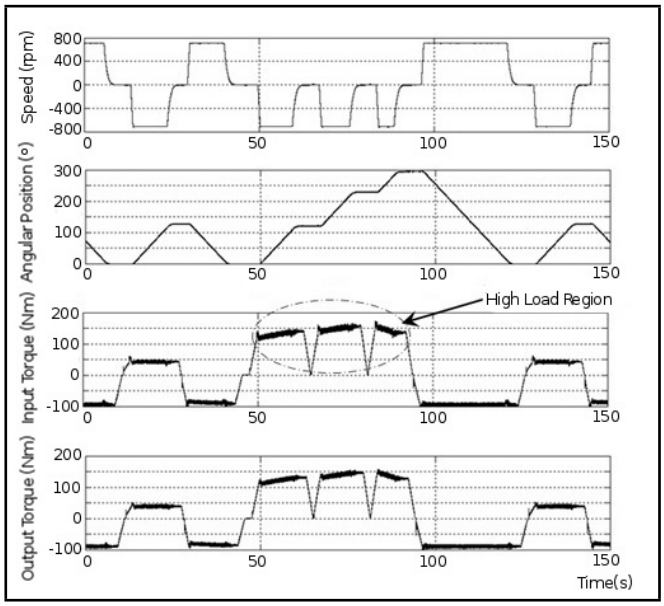

Figure 6. Type 3 load cycle profile.

tached to an NI USB 6009 data acquisition device. This digital data was filtered, windowed, and stored in the computer using Dasylab version 10.0, and finally it was exported for its final manipulation in Matlab R2010A. Other than the vibration data, various parameters were monitored and stored at the same time and with the same sampling frequency: angular position of the input shaft, input and output torque, and shaft speed.

The experiment started running on 19 July 2010 and the vibration measurements were taken on the 19 August 2010, 22 August 2010, and finally on 24 August 2010. For each measurement case, a total 1,048,569 points were acquired at a sampling rate of 5 kHz, which resulted in a measurement length of approximately 3.5 minutes; sufficiently long to cover a whole loading cycle. The stored data was then analysed, selecting groups of 8,192 data samples in the region of constant speed where maximum load was applied (Fig. 6). After a preliminary data analysis it was decided to always use the signal acquired by the third channel in the next steps of the analysis. This signal comes from the accelerometer which measures acceleration in the horizontal plane, and the characteristics found in the signal spectrum were representative of what was observed in the other channels.

The visibility of the main signal components is usually measured using the signal-to-noise ratio (SNR). This concept is widely used in electronics to evaluate the performance of dif-

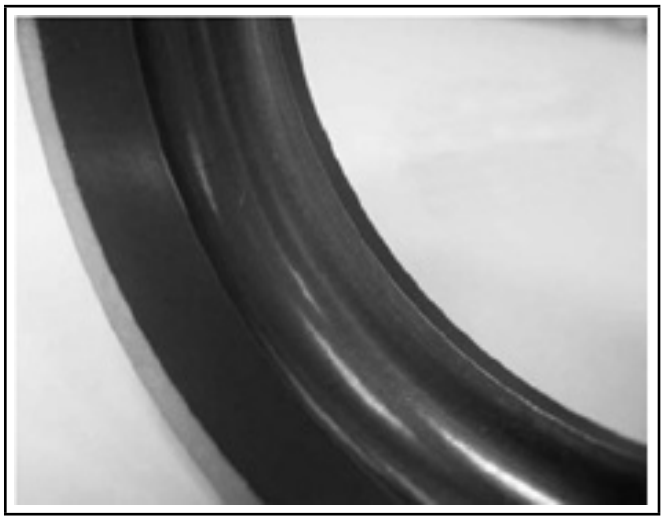

Figure 7. Detail of bearing outer race after one month.

ferent electronic devices such as amplifiers or radio receivers because it gives a measure of the signal quality. In those applications, the signal-to-noise ratio is calculated as the ratio between the power of the signal and the power of the background noise. Another definition of SNR is the ratio between the average amplitude of the main signal components μ, and the standard deviation of the background noise σ, which is equivalent to the reciprocal of the coefficient of variation.[34] This alternative definition is used in those applications where it is difficult to differentiate between the main signal and the background noise such as image processing, and this definition was employed in this investigation. The average amplitude of the main signal components was calculated in each case as the average amplitude of the visible peaks associated with the characteristic defect frequencies (Table 2), while the rest of the components with significant lower amplitude were considered as background noise. In order to estimate the average amplitude of the main signal components, the amplitude attached to each characteristic frequencies of the rig (Table 2) and its harmonics, was calculated for each spectrum. Obviously, because not all the possible defects were present at all times, it was necessary to determine whether there is a visible peak at each of those defect frequencies or not for each measurement. The assumption made was to consider main signal components only those peaks whose amplitude in the spectrum is at least 3 times the average amplitude across the whole frequency range. This average was calculated excluding the amplitudes related with the defect frequencies. Using this procedure, it was possible to separate the main peaks in the spectrum attached to the known defect frequencies and the rest of the components in the spectrum, considered as background noise. According to this definition, each case that studied the improvement in the signal-to-noise ratio was measured as a percentage comparing the SNR of the manipulated signal against the SNR of the raw signal.

4. RESULTS OBTAINED

Once the experiment was carried out, the data acquired was processed using the methodologies mentioned in Section 2. The results obtained for each measurement are plotted in this section with the following format:

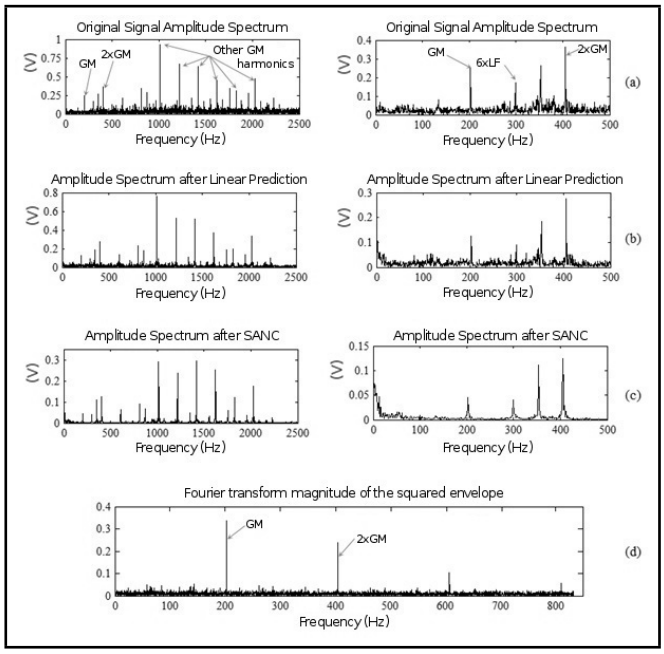

Figure 8. Results obtained from the first observation (19/08/10)

a) Amplitude spectrum of the original signal

b) Amplitude spectrum of the signal obtained by LP

c) Amplitude spectrum of the signal obtained by SANC

d) Magnitude of the squared envelope of the signal obtained by filtration in the frequency band of the maximum SK

The spectrums of the original signal and the signals obtained by LP and SANC are represented twice. The left plot corresponds to the spectrum covering a frequency range of 0–2500 Hz which contains the gear mesh components and its harmonics. The right plot covers the region of 0–500 Hz, where it is easier to identify the typical defect frequencies. The available frequency range of the squared envelope of the signal obtained by filtration after the kurtosis analysis depends on the filter parameters, different for each analysis. The kurtograms of the different observations and the main information extracted taken can be seen in Annex 1.

4.1. First Observation (19/08/2010)

For this observation, the LP analysis (Fig. 8(b)) was performed using 200 past samples for each prediction, and the parameters selected for the self-adaptive filter (Fig. 8(c)) were: delay $\Delta = 100$ samples, filter order $H = 1000$, and forgetting factor $\mu = 0.00001$. The maximum kurtosis found was 2.4, at a frequency band centred in 2083.33 Hz and a bandwidth of 833.3 Hz.

4.2. Second Observation (22/08/2010)

For the second observation, the LP analysis (Fig. 9(b)) was performed using 200 past samples for each prediction, and the parameters selected for the self-adaptive filter (Fig. 9(c)) were: delay $\Delta = 500$ samples, filter order $H = 1000$ and forgetting factor $\mu = 0.00005$. The maximum kurtosis found was 2.4 at a frequency band centred in 2083.33 Hz and a bandwidth of 833.3 Hz.

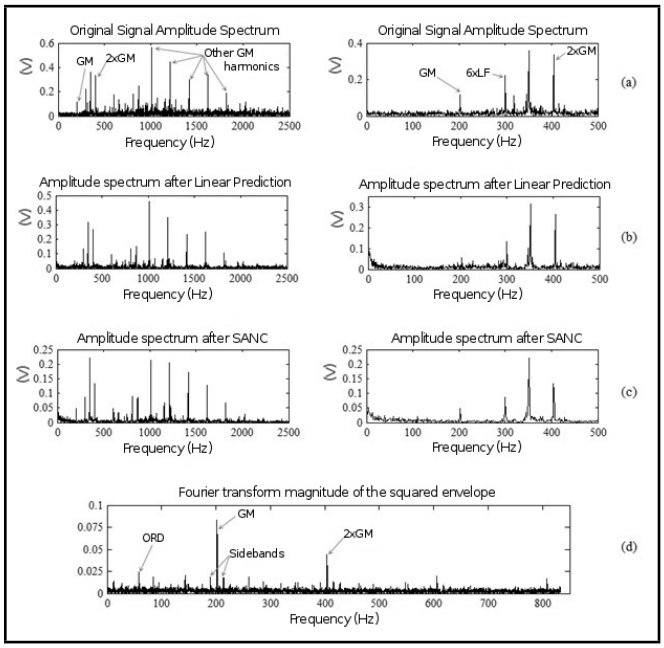

Figure 9. Results obtained from the second observation (22/08/10)

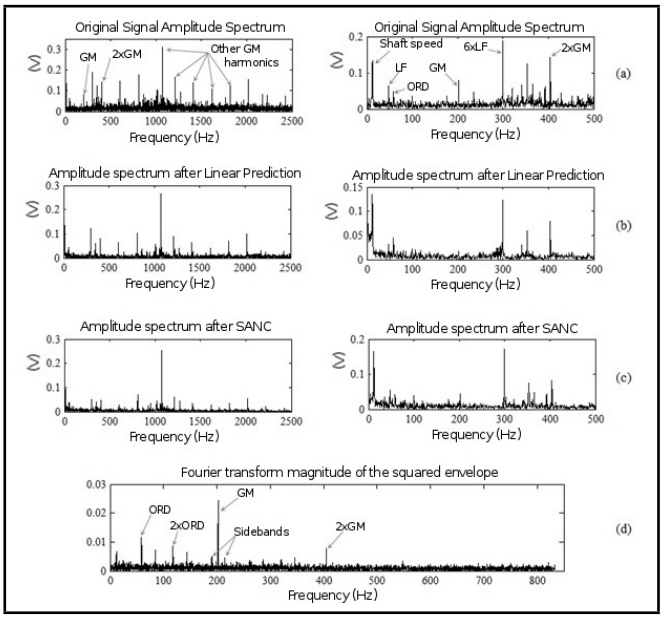

Figure 10. Results obtained from the third observation (24/08/10).

4.3. Third Observation (24/08/2010)

For the third observation, the LP analysis (Fig. 10(b)) was performed using 200 past samples for each prediction, and the parameters selected for the self-adaptive filter (Fig. 10(c)) were: delay $\Delta = 500$ samples, filter order $H = 1000$, and forgetting factor $\mu = 0.0001$. The maximum kurtosis found was 1.7, at a frequency band centred in 2083.33 Hz and a bandwidth of 833.3 Hz.

5. RESULTS AND DISCUSSION

The first measurement (19/08/10, Fig. 8) was acquired one month after the start of the experiment, which corresponds approximately to 24% of the expected bearing life. The spectrum of the original signal is clearly dominated by the gear mesh frequency ($\sim$202 Hz) and its harmonics. However, looking closely to the lower frequencies (the right column) it is possible to see a peak around 352 Hz, which is close to the 6^{th} harmonic of the outer race defect frequency (ORDF), but any defect in the outer race at this point was ruled out by visual inspection (see Fig. 7). The presence of this peak is attributed to a natural frequency of the structure or a consequence of deformation due to the three-point clamping during grinding the outer ring, and it will be present in all the stages of the experiment. There is also a component at 300 Hz, which corresponds to the 6^{th} harmonic of the 50 Hz line frequency (LF). This was corroborated by the fact that this peak appears even for those analyses carried out using data from the load cycle region where the motor speed was 0, indicating that this is a parasite component coming from the electrical grid.

From the analysis and observations of Fig. 8, background noise was reduced by LP and especially by SANC, increasing clearly the signal-to-noise ratio compared with the original signal, which are 2.6% and 42.9%, respectively (see Table 4), and facilitating the identification of the different signal components. The amplitude of the main peaks in the frequency spectrum were also reduced in magnitude, but this is not significant in terms of component identification because the signal contains the same main components at a better signal-to-noise ratio. No new peaks masked by the background noise were identified. The envelope obtained after the signal filtration at the maximum kurtosis frequency band shows clearly that the signal is dominated by the gear mesh frequency, but at this moment it does not provide any information of an incipient fault in the system.

The original spectrum of the second measurement taken three days after the first one (see Fig. 9) shows more or less the same components noted in the first observation, with the difference being that there is a reduction in the amplitude of the peaks, and the background noise is slightly lower. No new signal components are identified by LP or SANC, despite the fact that the background noise reduction is considerable, with an improvement of the 14.4% and 16.5%, respectively, in the signal-to-noise ratio in comparison with the original signal (see Table 4). The most interesting result of this analysis is the signal envelope obtained after the filtration at the maximum kurtosis band: apart from the typical gear mesh frequency and harmonics, it is possible to identify a new peak at the frequency of 58.4 Hz, indicating an incipient fault in the outer race of the bearing, in addition to sidebands around the gear mesh frequency at 190.2 Hz and 214 Hz. The distance between them and the gear mesh frequency is approximately 12 Hz, the shaft speed. It is important to emphasize the fact that (d) in Figs. 7, 8, and 9 represents the spectrum of the squared envelope of the filtered signal, not the spectrum of the filtered signal itself.

On 24 August 2010, the last data capture was performed (see Fig. 10). The first observation to note is that the amplitude of the different components is lower in this case. This is due to the fact that this measurement was done during a loading cycle type where the maximum transmitted torque was lower (40 Nm) than in the previous measurements (125 Nm). Even under these low torque conditions and despite the reduction in amplitude, all previously noted peaks were evident in the spectrum, in addition to a clear peak at 58.8 Hz, indicating the defect in the outer race of the bearing. Moreover, several sidebands around the harmonics of the gear mesh frequency,

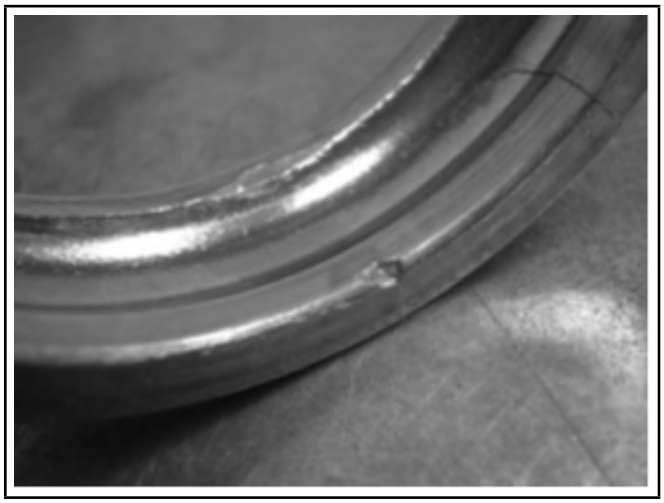

Figure 11. Bearing outer race degradation after 36 days.

Table 4. Maximum Kurtosis location.

Observation	Method	μ	σ	SNR
1	Original	0.2001	0.0190	10.5315
	LP	0.1004	0.0093	10.8054
	SANC	0.0612	0.0041	15.0496
	SK	0.0570	0.0054	10.6368
2	Original	0.1304	0.0120	10.8667
	LP	0.0701	0.0056	12.4314
	SANC	0.0548	0.0043	12.6596
	SK	0.0158	0.0014	11.1926
3	Original	0.0886	0.0087	10.18391
	LP	0.0487	0.0040	12.1750
	SANC	0.0353	0.0023	15.4082
	SK	0.0081	0.0008	9.6747

separated by the shaft frequency, were noted, showing that probably the bearing failure was causing a shaft misalignment, which affected the gear mesh. The spectrum of the squared envelope showed the peak at 58.8 Hz and a second harmonic of it at 117.9 Hz, indicating the fault in the outer race that was confirmed after by visual inspection of the component (Fig. 11).

6. CONCLUSION

This investigation shows the results of the application of three different vibration-based analysis methodologies for bearing diagnosis: LP, SANC, and SK together with envelope analysis. These techniques are typically used for applications where strong background noise masks the mechanical signature of a machine, making the identification of the fault source challenging. This is the case of the experiment presented in this investigation. LP, and particularly, the SANC showed its capability to reduce the background noise and facilitate the identification of the different components in the signal spectrum, but in this specific application they did not identify the defect on a bearing earlier than the SK.

The latter technique demonstrated the ability to identify the defect earlier than all other methods. This method is thus a very powerful tool for the early detection of faults in bearings, even for those applications where strong background noise from other sources in the machine masks the characteristic fault components in the frequency domain.

ACKNOWLEDGEMENTS

Financial support from the Marie Curie FP7-ITN project "Energy savings from smart operation of electrical, process and mechanical equipment– ENERGY-SMARTOPS," Contract No: PITN-GA-2010-264940 is gratefully acknowledged

REFERENCES

[1] Ho, D. and Randall, R. B. Optimization of bearing diagnostic techniques using simulated and actual bearing fault signals, *Mechanical Systems and Signal Processing*, **14** (5), 763–788, (2000).

[2] Tan, C. C. An Adaptive Noise Cancellation Approach for Condition Monitoring of Gear Box Bearings, *International Tribology Conference, no 87/18*, Melbourne, Victoria, 360–365, (1987).

[3] Randall, R. B. and Antoni, J. Rolling element bearing diagnostics – A tutorial, *Mechanical Systems and Signal Processing*, **25** (2), 485–520, (2011).

[4] Behzad, M., Bastami, A. R. and Mba, D. Rolling bearing fault detection by short-time statistical features, *Proceedings of the Institution of Mechanical Engineers, Part E: Journal of Process Mechanical Engineering*, **226** (3), 229–237, (2012).

[5] Li, H., Zhang, Y. and Zheng, H. Hilbert-Huang transform and marginal spectrum for detection and diagnosis of localized defects in roller bearings, *Journal of Mechanical Science and Technology*, **23** (2), 291–301, (2009).

[6] Li, F., Meng, G., Ye, L. and Chen, P. Wavelet transform-based higher-order statistics for fault diagnosis in rolling element bearings, *JVC/Journal of Vibration and Control*, **14** (11), 1691–1709, (2008).

[7] Makhoul, J. Linear Prediction: A Tutorial Review, *Proceedings of the IEEE*, **63** (4), 561–580, (1975).

[8] Widrow, B., Glover Jr., J. R. and McCool, J. M. Adaptive noise cancelling: principles and applications, *Proceedings of the IEEE*, **63** (12), 1692–1716, (1975).

[9] Da Silva, S. and Dias Junior, M. Statistical damage detection in a stationary rotor systems through time series analysis, *Latin American Applied Research*, **37** (4), 243–246, (2007).

[10] Dron, J. -., Rasolofondraibe, L., Chiementin, X. and Bolaers, F. A comparative experimental study on the use of three denoising methods for bearing defect detection, *Meccanica*, **45** (2), 265–277, (2010).

[11] Lu, B., Nowak, M., Grubic, S. and Habetler, T. G. An adaptive noise-cancellation method for detecting generalized roughness bearing faults under dynamic load conditions, *2009 IEEE Energy Conversion Congress and Exposition, ECCE 2009*, 1091, (2009).

[12] Sawalhi, N. and Randall, R. B. Helicopter gearbox bearing blind fault identification using a range of analysis techniques, *Australian Journal of Mechanical Engineering*, **5** (2), 157–168, (2008).

[13] Sui, W. and Zhang, D. *DWT-based adaptive filter and its application on canceling noise in mechanical signals*, (2010).

[14] Wang, W. Autoregressive model-based diagnostics for gears and bearings, *Insight: Non-Destructive Testing and Condition Monitoring*, **50** (8), 414–418, (2008).

[15] Patel, V. N., Tandon, N. and Pandey, R. K. Improving defect detection of rolling element bearings in the presence of external vibrations using adaptive noise cancellation and multiscale morphology, *Proceedings of the Institution of Mechanical Engineers, Part J: Journal of Engineering Tribology*, **226** (2), 150–162, (2012).

[16] Antoni, J. The spectral kurtosis: A useful tool for characterising non-stationary signals, *Mechanical Systems and Signal Processing*, **20** (2), 282–307, (2006).

[17] Antoni, J. and Randall, R. B. The spectral kurtosis: Application to the vibratory surveillance and diagnostics of rotating machines, *Mechanical Systems and Signal Processing*, **20** (2), 308–331, (2006).

[18] Antoni, J. Fast computation of the kurtogram for the detection of transient faults, *Mechanical Systems and Signal Processing*, **21** (1), 108–124, (2007).

[19] Chen, J., Zi, Y., He, Z. and Yuan, J. Improved spectral kurtosis with adaptive redundant multiwavelet packet and its applications for rotating machinery fault detection, *Measurement Science and Technology*, **23** (4), (2012).

[20] Li, H., Zheng, H. and Tang, L. Bearing fault diagnosis based on kurtogram of dual-tree complex wavelet packet transform, *Zhendong yu Chongji/Journal of Vibration and Shock*, **31** (10), 13–18, (2012).

[21] Bechhoefer, E., Kingsley, M. and Menon, P. Bearing envelope analysis window selection using spectral kurtosis techniques, *2011 IEEE International Conference on Prognostics and Health Management, PHM 2011 - Conference Proceedings*, (2011).

[22] Lei, Y., Lin, J., He, Z. and Zi, Y. Application of an improved kurtogram method for fault diagnosis of rolling element bearings, *Mechanical Systems and Signal Processing*, **25** (5), 1738–1749, (2011).

[23] Wang, Y. and Liang, M. An adaptive SK technique and its application for fault detection of rolling element bearings, *Mechanical Systems and Signal Processing*, **25** (5), 1750–1764, (2011).

[24] Su, W., Wang, F., Zhang, Z., Guo, Z. and Li, H. Application of EMD denoising and spectral kurtosis in early fault diagnosis of rolling element bearings, *Zhendong yu Chongji/Journal of Vibration and Shock*, **29** (3), 18–21, (2010).

[25] Yule, G. U. On a method of investigating periodicities in disturbed series, with special reference to Wolfer's sunspot numbers, *Philosophical Transactions of the Royal Society of london*, **226-A**, 267–298, (1927).

[26] Randall, R. B. 3.6.3 Linear Prediction, in John Wiley and Sons (ed.) *Vibration-based condition monitoring: Industrial, aerospace and automotive applications*, 2011th ed, Wiley, Singapore, 122–125, (2011).

[27] Ljung, L. 10.1 Linear Regressions and Least Squares, in Pentrice-Hall (ed.) *System identification: Theory for the user, 2nd ed, Pentrice-Hall, New Jersey*, 321–324, (1999).

[28] Chaturvedi, G. K. and Thomas, D. W. Bearing fault detection using adaptive noise cancelling, *Trans.ASME J.Mech.Des.*, **104** (2), Apr. 1982, 280–289, (1982).

[29] Antoni, J. and Randall, R. B. Unsupervised noise cancellation for vibration signals: Part I - Evaluation of adaptive algorithms, *Mechanical Systems and Signal Processing*, **18** (1), 89–101, (2004).

[30] Ho, D. and Randall, R.B. Effects of time delay, order of FIR filter and convergence factor on self adaptive noise cancellation, *Fifth International Congress on Sound and Vibration*, Adelaide, 945–952, (1997).

[31] Randall, R. B. 3.1. Probability Distribution and Density, in John Wiley and Sons (ed.) *Vibration-based condition monitoring: Industrial, aerospace and automotive applications*, Wiley, Singapore, (2011), 63–66.

[32] Dwyer, R. F. Detection of Non-Gaussian Signals by Frequency Domain Kurtosis Estimation, *ICASSP, IEEE International Conference on Acoustics, Speech and Signal Processing - Proceedings*, **2**, 607, (1983).

[33] Randall, R. B. 5.3 Spectral Kurtosis and the Kurtogram, in John Wiley and Sons (ed.) *Vibration-based condition monitoring: Industrial, aerospace and automotive applications*, Wiley, Singapore, (2011), 122–125.

[34] Smith, S. W. *The scientist and engineer's guide to digital signal processing*, 1st ed, California Technical Publishing, California, (1997).

ANNEX 1: INFORMATION PROVIDED BY THE KURTOGRAM

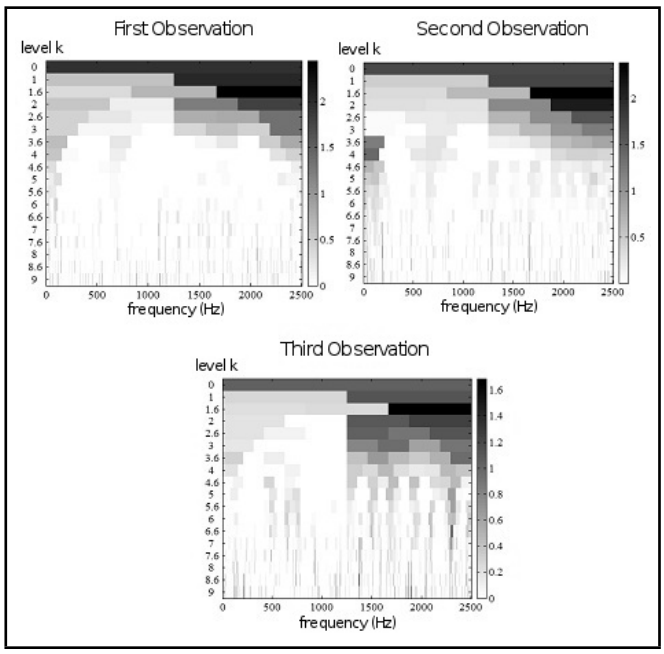

Figure 12. Kurtograms of the different observations.

Table 5. Maximum Kurtosis location.

Observation	Fc(Hz)	Δf(Hz)	K max	Frequency Band(Hz)
1	2083.33	833.3	2.4	1666.7-2500
2	2083.33	833.3	2.4	1666.7-2500
3	2083.33	833.3	1.7	1666.7-2500